

Hydrothermal Synthesis and Electrochemical Performance of Amorphous SiO₂ Nanospheres/Graphene Composites

Youwen Yang^{1*}, Yuanhao Gao², Jiguang Liu^{1#}, Xiaogang Fang¹

¹School of Materials Science and Engineering, Hefei University of Technology, Hefei, China

²School of Chemistry and Chemical Engineering, Hefei University of Technology, Hefei, China

Email: *hfutyw@hfut.edu.cn, #jiguangliu@163.com

How to cite this paper: Yang, Y.W., Gao, Y.H., Liu, J.G. and Fang, X.G. (2017) Hydrothermal Synthesis and Electrochemical Performance of Amorphous SiO₂ Nanospheres/Graphene Composites. *Materials Sciences and Applications*, 8, 959-965. <https://doi.org/10.4236/msa.2017.813070>

Received: October 21, 2017

Accepted: December 5, 2017

Published: December 8, 2017

Copyright © 2017 by authors and Scientific Research Publishing Inc. This work is licensed under the Creative Commons Attribution International License (CC BY 4.0).

<http://creativecommons.org/licenses/by/4.0/>



Open Access

Abstract

The exceptional mechanical and electrical nature of graphene makes it a viable candidate for enhancing the effectiveness of electrode material. In recent years, Graphene based SiO₂ nanocomposites is a research hot topic of anode materials in lithium-ion batteries. In this paper, the amorphous SiO₂ nanospheres/graphene composite was synthesized by hydrothermal method. Amorphous SiO₂ is attached to the surface of graphene with a spherical structure and its average diameter is about 200 nm. The weight of SiO₂ in the nanospheres composite is about 43%. Electrochemical tests showed that the amorphous SiO₂ nanospheres/graphene composite exhibited the first charge and discharge capacity is respectively 329.5 mAhg⁻¹ and 444.1 mAhg⁻¹, and remain at 257.8 mAhg⁻¹ and 274.6 mAhg⁻¹ for 50th cycles at a current density of 200 mA g⁻¹. The amorphous SiO₂ nanospheres/graphene composite structure is novelty and the results are of great significance to the preparation and application of new anode materials.

Keywords

Amorphous SiO₂ Nanospheres, Graphene, Anode, Cycle Performance

1. Introduction

As one kind of acidic non-metallic oxide, Silicon dioxide (SiO₂) is mainly in the form of crystalline and amorphous. The chemical properties of crystalline SiO₂ are relatively stable, while the structure of amorphous SiO₂ is irregularly continuous network one, which has higher activity than crystalline SiO₂. Due to its low conductivity, SiO₂ had been considered difficult to use as electrode material.

However, previous studies have proposed that compared with crystalline silicon oxide, amorphous SiO₂ is favored in industry with respect to cycling stability [1]. And the size and crystal structure of the SiO₂ have a significant impact on its electrochemical performance [2] [3]. SiO₂ nanoparticles were found to react with Li in the voltage range of 0 - 1 V and the n-Si/Li system has a lower and essentially constant electrochemical potential relative to Li/Li⁺, which is advantageous for use as anode materials in Li-based batteries [4]. In order to explore the application of SiO₂ in electrode materials, graphene based SiO₂ nanocomposites have recently been studied in detail for applications in lithium-ion batteries, e.g., SiO₂ nanoparticles/graphene [5] [6], SiO₂ nanospheres/graphene [7] [8] and ternary composites [9] [10]

Herein, we employed the hydrothermal method to fabricate amorphous SiO₂ nanospheres/grapheme (a-SiO₂@G) nanocomposite for the first time, in which the diameter of SiO₂ is about 200 nm. The synthesis process and the structure character of a-SiO₂@G were studied in detail. Meanwhile, the electrochemical performance of a-SiO₂@G as anode for LIBs has also been evaluated.

2. Experimental

Graphite oxide (GO) was prepared from powdered flake graphite (Qingdao Jinri Graphite Co., Ltd, China) by the modified Hummer's method. Sodium dodecyl sulfate (SDS, AR), Tetraethylorthosilicate (TEOS, AR) and NaOH (AR) were purchased from Sinopharm Chemical Reagent Co. Ltd., China. All reagents were used without further purification. The obtained GO (30 mg) was added into distilled water (3 ml) with ethanol (30 ml) respectively, 25 mg sodium dodecyl sulfate was then added, followed by 1 h ultra-sonication to make a homogeneous suspension. Then, 25 ml TEOS and 3 mg NaOH were added into the suspension respectively. After 15 min of ultrasonic treatment, the mixture was dissolved in the mixture under magnetic stirring at room temperature for 2 h. Finally, the resulting solution was transferred to 100 ml Teflon-lined stainless steel autoclave for the hydrothermal reaction. The autoclave was sealed and heated at 160 °C for 12 h in an electrical oven. After heating treatment, the autoclave was cooled to room temperature. Black products were obtained by centrifugation, washed with distilled water 3 times prior to be dried in vacuum at 60 °C for 12 h.

The products were characterized by X-ray diffraction (XRD, RigakuD/ MAX-RC, Japan) with Cu K α radiation ($\lambda = 1.518 \text{ \AA}$), as well as field emission scanning electron microscopy (FE-SEM, HITACHISU8020, Japan), and transmission electron microscopy (TEM, JEOLJEM-2100F, Japan). Raman spectroscopy was used to estimate the bond structure of the products (Raman, Evolution, France). The carbon mass ratio was investigated by thermal gravimetric analysis (TGA, STA449F3, Germany) from 25 °C to 1000 °C. A Nova 2200e specific surface area tester (USA) was used to measure surface area of samples using Braunauer-Emmet-Teller (BET,) method.

To evaluate the electrochemical performance of the composites, the samples

were mixed with acetylene black (Lion Co., Japan) and polyvinylidene fluoride (PVDF, Defulong anti-corrosion equipment Co. Ltd., China) in a weight ratio of 7:2:1 in N-methylpyrrolidinone (NMP, Maiqi Technology Co. Ltd., China) solvent. Then, the slurry was uniformly cast on a copper foil and dried at 90°C under vacuum for 12 h. The coin cells were assembled inside an argon-filled glovebox using lithium metal foil as the counter electrode and the polypropylene as the separator. The electrolyte was 1 M LiPF₆ dissolved in ethylene carbonate and dimethyl carbonate (LiPF₆/EC + DEC, Huarong New Chemical Materials Co., China) solvent (1:1 volume ratio). Finally, galvanostatical charge/discharge were carried out at a current rate of 200 mA g⁻¹, in a potential range of 0.01 V - 3.00 V (vs. Li⁺/Li) on a Land CT2001A system (Neware Technology Co. Ltd. China)

3. Results and Discussion

Morphological investigations have been carried out to understand the shape and structure of a-SiO₂@G composites. **Figure 1(a)** illustrates that the prepared SiO₂ shows spherical shape, monodispersed nanospheres with the diameter about 200 nm. The TEM image of graphene is displayed inset of **Figure 1(a)** and it can be seen that the graphene in the nanocomposite structure is an obvious lamellar structure with many folds on its surface. The semi-transparent graphene sheets with anchored SiO₂ nanospheres are clearly visible in **Figure 1(b)**, thereby confirming the attachment of SiO₂ nanospheres to the surface of graphene.

The crystalline of prepared samples is analyzed in the range of 5° - 80° as depicted in. From the natural graphite XRD pattern of graph (**Figure 2(a)**), it is easy to distinguish the characteristic diffraction peaks of natural graphite, and the Bragg diffraction angles 2θ are located at 26.4° and 43.3°, respectively, corresponding to (002) and (100) two characteristic peaks. It can be seen that GO exhibits the typical (002) reflection at $2\theta = 10.9^\circ$. According to Prague's law ($2d \sin \theta = n\lambda$), the corresponding interlayer distance is calculated to be 0.8117 nm, which is bigger than the previous works [11]. We think that a large amount of oxygen-containing groups are interposed between the carbon layers during the oxidation of the natural graphite, resulting in an increase in the interlayer spacing of the graphite. The diffraction angle of the diffraction peak in the XRD pattern shifted from 11.54° to 10.9°. It is further explained that the oxidation of

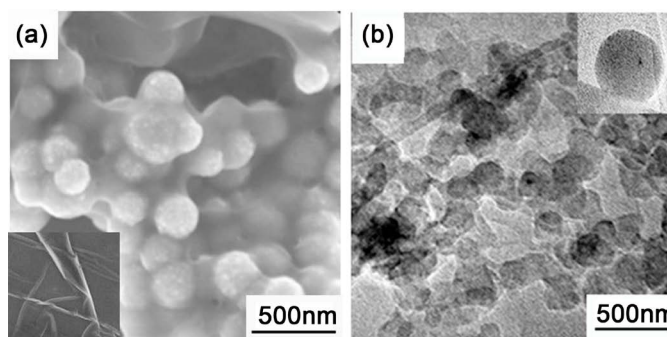


Figure 1. The FE-SEM (a) and TEM (b) images of a-SiO₂@G composites.

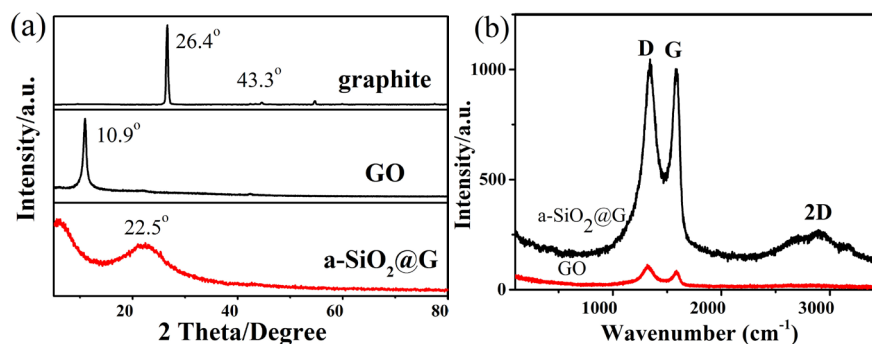


Figure 2. The XRD patterns (a) of graphite, GO, a-SiO₂@G composites and the Raman spectra of GO, a-SiO₂@G composites.

graphite prepared by the improved Hummers method is highly oxidized. The XRD pattern of the a-SiO₂@G composites has a broadening peak between $2\theta = 15^\circ$ and 30° . The broad XRD peak at $2\theta = 22.5^\circ$ matches well with that of the SiO₂ spheres [7] and indicates that the structure is amorphous.

The structure of GO and a-SiO₂@G composites was further studied by Raman spectra in **Figure 2(b)**. Both Raman spectra of GO and a-SiO₂@G composites exhibit two obvious peaks corresponded to the disordered D band G band of carbon. The GO has the D-band and G-band located at 1323 cm^{-1} and 1586 cm^{-1} respectively. The a-SiO₂@G composites have the D-band and G-band located at 1343 cm^{-1} and 1584 cm^{-1} respectively. As we known, the D peak is caused by defects of sp^2 carbon atom structure rGO, while G peak is related to the in-plane vibration of sp^2 carbon atom [12]. We can see that the intensity ratio of the D to the G band (I_G/I_D) of a-SiO₂@G composites (1.044) is lower than 1.309 of GO, indicating that the defect of graphene in a-SiO₂@G composites was significantly reduced compared with that of GO. The band at 2893 cm^{-1} corresponding to the 2D peak indicates the multilayer structure of rGO in the a-SiO₂@G composites [13]. According to the empirical formula:

$$w_G = 1581.6 + 11 / (1 + n^{1.6})$$

where w_G is the value of G peak (1584), we can get that $n = 2.2$. It also means that the graphene in a-SiO₂@G composite structure has fewer layers and higher quality.

To determine the amorphous carbon mass ratio in the a-SnO₂@G composites, thermogravimetric analysis (TGA) is carried out with a temperature ramp of $10^\circ\text{C}/\text{min}$ and nitrogen is used as protective gas. As shown in **Figure 3(a)**, a-SnO₂@G composites began to lose weight even under 100°C due to the thermal instability of GO, the occurrence of a weight loss of about 3% is attributed to release of the absorbed gases or moisture on the surface of the a-SiO₂@G [14]. From 100°C to 300°C , the TGA curve declines slowly because of the decomposition of a small amount of oxygen containing functional groups of graphene [15]. The weight loss at $300^\circ\text{C} - 900^\circ\text{C}$ is attributed to decomposition of graphene and the ratio of absorbed water, rGO and the SiO₂ in the nanospheres composite is ~3%, ~54%, and ~43% respectively.

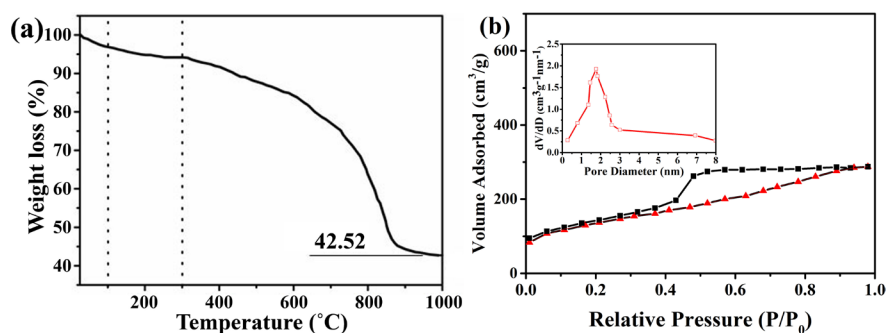


Figure 3. TGA curve and nitrogen adsorption-desorption isotherm of a-SiO₂@G composites.

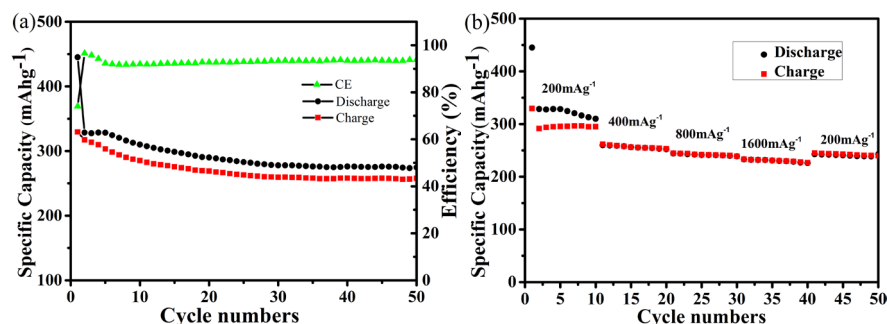


Figure 4. The cycle performance, columbic efficiency (a) and rate performance (b) of a-SiO₂@G composites.

Figure 3(b) shows the nitrogen adsorption-desorption curves and pore size distribution of the a-SiO₂@G composites. The N₂ adsorption-desorption isotherm for a-SiO₂@G is of type IV classification with H1 hysteresis ($P/P_0 = 0.4 - 0.90$), indicating that there are a lot of mesopores existing in the composites [16]. As shown in the **Figure 3(b)** (inset), the narrow pore size distributions appear in the a-SiO₂@G curves with the maximum value located at 2 nm from the adsorption isotherm. The a-SiO₂@G composites exhibit higher surface area ($S_{\text{BET}} = 480.880 \text{ m}^2 \text{ g}^{-1}$) and its pore average diameter is 2.587 nm by the BET method.

The cycle performance and columbic efficiency (CE) of a-SiO₂@G composites are exhibited in **Figure 4(a)**. It can be seen that the a-SiO₂@G composite demonstrates a relatively high initial discharge and charge capacity of 444.1 mAhg^{-1} and 329.5 mAhg^{-1} respectively. The high initial CE (74.2%), which is higher than SiO₂@C composites [17] [18], is attributed to the large specific surface area and porous structure of the a-SiO₂@G. The cyclic performance of the a-SiO₂@G composites is relatively stable, and the efficiency of CE has risen to 96.4% in the second cycle. After 50 cycles, the irreversible capacity decreased to 257.8 mAhg^{-1} and the CE is 93.8%. As shown in **Figure 4(b)**, the a-SiO₂@G anode exhibits specific capacities of 329.5 , 261.6 , 244.5 and 239.8 mAhg^{-1} , at rates of 200, 400, 800 and 1600 mA g⁻¹ respectively. The specific capacity well recovers to 246 mAhg^{-1} when the rate is decreased from 1600 mA g⁻¹ to 200 mA g⁻¹. The higher surface area of the a-SiO₂@G composites is beneficial to the full contact with the electrolyte and the porous structure is expected to offer enough

open channels as passage of electrolyte for the electrochemical reactions and suppressed the volume changes, thus accelerating the diffusion rate of lithium ions.

4. Conclusion

In summary, high surface area a-SiO₂@G composite has been successfully prepared by a hydrothermal technique and investigated as anode materials for LIBs. The amorphous SiO₂ nanospheres with a diameter of 200 nm were embedded in the rGO sheets, building a stable composite structure. And the graphene in a-SiO₂@G composite structure has fewer layers and higher quality. Electrochemical measurement displays that the improved cycling performance is attributed to two main factors, such as large surface areas and porous structures.

Acknowledgements

We greatly acknowledge partial financial support by Anhui science and technology major projects (15czz04124) and Enterprise cooperation project (W2016JSKF030, W2017JSKF0071).

References

- [1] Kim, J.Y., Nguyen, D.T., Kang, J.S. and Song, S.W. (2015) Facile Synthesis and Stable Cycling Ability of Hollow Submicron Silicon Oxide-Carbon Composite Anode Material for Li-Ion Battery. *Journal of Alloys and Compounds*, **633**, 92-96. <https://doi.org/10.1016/j.jallcom.2015.01.309>
- [2] Yu, Y., Zhang, J., Xue, L., Huang, T. and Yu, A. (2011) Carbon-Coated SiO₂ Nanoparticles as Anode Material for Lithium ion Batteries. *Journal of Power Sources*, **196**, 10240-10243. <https://doi.org/10.1016/j.jpowsour.2011.08.009>
- [3] Guo, B., Shu, J., Wang, Z., Yang, H., Shi, L. and Liu, Y. (2008) Electrochemical Reduction of Nano-SiO₂ in Hard Carbon as Anode Material for Lithium ion Batteries. *Electrochemistry Communications*, **10**, 1876-1878. <https://doi.org/10.1016/j.elecom.2008.09.032>
- [4] Gao, B., Sinha, S., Fleming, L. and Zhou, O. (2001) Alloy Formation in Nanostructured Silicon. *Advanced Materials*, **13**, 816-819. [https://doi.org/10.1002/1521-4095\(200106\)13:11<816::AID-ADMA816>3.0.CO;2-P](https://doi.org/10.1002/1521-4095(200106)13:11<816::AID-ADMA816>3.0.CO;2-P)
- [5] Nguyen, D.T., Nguyen, C.C., Kim, J.S., Kim, J.Y. and Song, S.W. (2013) Facile Synthesis and High Anode Performance of Carbon Fiber-interwoven Amorphous Nano-SiO_x/Graphene for Rechargeable Lithium Batteries. *ACS Applied Materials & Interfaces*, **13**, 816-819. <https://doi.org/10.1021/am4034763>
- [6] Lv, L., Huang, L., Zhu, P., Li, G., Zhao, T., Long, J.P., Sun, R. and Wong, C.P. (2017) SiO₂ Particle-Supported Ultrathin Graphene Hybrids/Polyvinylidene Fluoride Composites with Excellent Dielectric Performance and Energy Storage Density. *Journal of Materials Science Materials in Electronics*, **28**, 13521-13531. <https://doi.org/10.1007/s10854-017-7191-0>
- [7] Iturbe-Ek, J., Andrade-Martínez, J., Gómez, R. and Rodríguez-González, V. (2015) A Functional Assembly of SiO₂ Nanospheres/Graphene Oxide Composites. *Materials Letters*, **142**, 75-79. <https://doi.org/10.1016/j.matlet.2014.11.149>
- [8] Wu, G.L., Wu, M.B., Wang, D., Yin, L.H., Ye, J.S., Deng, S.Z., Zhu, Z.Y., Ye, W.J. and Lia, Z.T. (2014) A Facile Method for In-situ, Synthesis of SnO₂/Graphene as a

- High Performance Anode Material for Lithium-Ion Batteries. *Applied Surface Science*, **315**, 400-406. <https://doi.org/10.1016/j.apsusc.2014.07.188>
- [9] Xiang, Z.M., Chen, Y.X., Li, J., Xia, X.H., He, Y.D. and Liu, H.B., (2017). Submicro-sized Porous SiO₂/C and SiO₂/C/graphene Spheres for Lithium ion Batteries. *Journal of Solid State Electrochemistry*, 21:2425-2432. <https://doi.org/10.1007/s10008-017-3566-7>
- [10] Choi, M., Yoon, I.H., Jo, I.H., Kim, H.S., Jin, B.S., Lee, Y.M. and Choi, W.K. (2015) The Effect of SiO₂ Nanoparticles in Li₃V₂(PO₄)₃/Graphene as a Cathode Material for Li-ion Batteries. *Materials Letters*, **160**, 206-209. <https://doi.org/10.1016/j.matlet.2015.07.085>
- [11] Vickery, J.L., Patil, A.J. and Mann, S. (2009) Fabrication of Graphene-Polymer Nanocomposites with Higher-Order Three-Dimensional Architectures. *Advanced Materials*, **160**, 206-209. <https://doi.org/10.1002/adma.200803606>
- [12] Arshad, A., Iqbal, J., Mansoor, Q. and Ahmad, I. (2017) Graphene/SiO₂ Nanocomposites: The Enhancement of Photocatalytic and Biomedical Activity of SiO₂ Nanoparticles by Graphene. *Journal of Applied Physics*, **121**, 244901. <https://doi.org/10.1063/1.4979968>
- [13] Xu, X.F., Zhang, H.Y., Chen, Y.M., Li, N., Li, Y.Y., and Liu, L.Y. (2016) SiO₂@SnO₂/Graphene Composite with a Coating and Hierarchical Structure as High Performance Anode Material for Lithium ion Battery. *Journal of Alloys & Compounds*, **677**, 237-244. <https://doi.org/10.1016/j.jallcom.2016.03.136>
- [14] Stankovich, S., Dikin, D.A., Piner, R.D., Kohlhaas, K.A., Kleinhammes, A., Jia, Y., Wu, Y., Nguyen, S.T. and Nguyen, R.S. (2007) Synthesis of Graphene-Based Nanosheets via Chemical Reduction of Exfoliated Graphite Oxide. *Carbon*, **45**, 1558-1565. <https://doi.org/10.1016/j.carbon.2007.02.034>
- [15] Huang, D., Yang, Z., Li, X.L., Zhang, L.L., Hu, J., Su, Y.J., Hu, N.T., Yin, G.L., He, D.N. and Zhang, Y.F. (2017). Three-dimensional Conductive Networks Based on Stacked SiO₂@Graphene Frameworks for Enhanced Gas Sensing. *Nanoscale*, **9**, 109-118. <https://doi.org/10.1039/C6NR06465E>
- [16] Meng, J.K., Cao, Y., Suo, Y., Liu, Y.S., Zhang, J.M. and Zheng, X.C. (2015) Facile Fabrication of 3D SiO₂@Graphene Aerogel Composites as Anode Material for Lithium ion Batteries. *Electrochimica Acta*, **176**, 1001-1009. <https://doi.org/10.1016/j.electacta.2015.07.141>
- [17] Kim, Y.K., Moon, J.W., Lee, J.G., Baek, Y.K. and Hong, S.H. (2014) Porous Carbon-Coated Silica Macroparticles as Anode Materials for Lithium ion Batteries: Effect of Boric Acid. *Journal of Power Sources*, **272**, 689-695. <https://doi.org/10.1016/j.jpowsour.2014.08.128>
- [18] Liu, X.L., Chen, Y.X., Liu, H.B. and Liu, Z.Q. (2017) SiO₂@C Hollow Sphere Anodes for Lithium-Ion Batteries. *Journal of Materials Science & Technology*, **33**, 239-245. <https://doi.org/10.1016/j.jmst.2016.07.021>